Diabetes, Metabolic Syndrome and Obesity

Dovepress
Taylor & Francis Group

Open Access Full Text Article

ORIGINAL RESEARCH

Causal Central Network Remodeling in Diabetic Neuropathy: An Integrated MR-fMRI Study

Xiya Li, Ling Gao

Department of Endocrinology and Metabolism, Renmin Hospital, Wuhan University, Wuhan, People's Republic of China

Correspondence: Ling Gao, Department of Endocrinology & Metabolism, Renmin Hospital of Wuhan University, Jiefang Road#238, Wuhan, 430060, People's Republic of China, Tel +86 15927469449, Fax +86 27 88042292, Email ling.gao@whu.edu.cn

Purpose: Diabetic peripheral neuropathy (DPN) is traditionally viewed as a peripheral disorder, yet emerging evidence implicates central nervous system (CNS) network dysfunction in its pathogenesis, though causal mechanisms remain incompletely understood.

Methods: Bidirectional two-sample Mendelian randomization (MR) analysis examined causal relationships between Resting-State Functional Magnetic Resonance Imaging (rs-fMRI) phenotypes (n=34,691) and DPN (n=96,474). For validation, amplitude of low-frequency fluctuation (ALFF) and functional connectivity (FC) analyses were conducted using rs-fMRI scans from DPN patients (n=16), diabetic controls without DPN (NDPN, n=24), and healthy controls (HC, n=20).

Results: Bidirectional MR demonstrated that: (a) reduced default mode-visual network connectivity causally elevates DPN risk (OR=0.61, P=0.04); (b) DPN promotes subcortical-cerebellar hyperconnectivity (OR=1.04, P=0.01). DPN patients exhibited significantly higher age, triglyceride levels, pain scores, and cognitive impairment relative to comparison groups (all P<0.001). Neuroimaging identified increased ALFF in the left superior frontal gyrus (LSFG) (AUC=0.79, P<0.05), which correlated positively with disease duration, accompanied by decoupled FC with the lingual gyrus but enhanced FC with the precuneus.

Conclusion: This study establishes DPN as a CNS-periphery integrated network disorder: genetic drivers disrupt default mode-visual integration, while compensatory subcortical-cerebellar hyperconnectivity stabilizes motor function via adaptive mechanisms. The LSFG emerges as a neuroadaptive hub, where elevated ALFF and connectivity reorganization (↓lingual gyrus/↑precuneus) reflect dynamic rebalancing between impaired basic vision and enhanced visuospatial processing. These findings redefine DPN pathogenesis beyond pure peripheral neurodegeneration, providing a theoretical foundation for early detection and circuit-targeted neuromodulation therapies.

Keywords: type 2 diabetes mellitus, diabetic peripheral neuropathy, low-frequency fluctuations, fMRI, Mendelian random analysis

Introduction

Diabetic peripheral neuropathy (DPN), a prevalent and debilitating chronic complication of diabetes mellitus, affects 67.6% of patients, with 57.2% experiencing painful DPN (PDPN).[1] Clinical manifestations range from asymptomatic numbness to intractable pain, frequently causing sleep disturbances, mood disorders, and reduced quality of life.[2,3] Notably, 25–50% of DPN patients develop neuropsychological impairments such as anxiety or depression, correlating with diminished psychomotor efficiency on cognitive assessments.[4]

Diabetes-associated central nervous system (CNS) pathology was initially documented through spinal cord atrophy and demyelination in 1960s autopsies,[5] while contemporary neuroimaging confirms structural CNS damage in DPN, including: spinal cord atrophy, somatosensory cortex grey matter loss, thalamic metabolic dysfunction, functional reorganization,[6,7] and altered neural activation patterns are evident across thalamic, insular, cingulate, and prefrontal regions.[8,9]

Additionally, DPN patients frequently exhibit visual impairments.[10] Subjects with DPN but without diabetic retinopathy (DR) exhibit increased macular thickness, reduced retinal nerve fiber layer (RNFL) thickness, and significantly impaired visual functions, suggesting optic nerve involvement via CNS mechanisms.[11] Animal models reveal CNS-mediated excitotoxicity and neurovascular changes contributing to visual pathway dysfunction,[12,13] while clinical studies indicate metformin improves retinal-brain axis abnormalities in diabetic retinopathy,[14] collectively establishing CNS-visual impairment associations.

Received: 27 February 2025
Accepted: 18 July 2025
Published: 9 August 2025

Traditional observational studies examining brain-DPN relationships face limitations from confounding and reverse causation. Mendelian randomization (MR) overcomes these by leveraging genetic variants as instrumental variables, effectively simulating randomized controlled trials to infer causality.[15]

Although electrophysiological techniques (eg, nerve conduction studies, NCS) are considered diagnostic gold standards for peripheral neuropathy, their sensitivity to central pathway impairment remains suboptimal.[16] Advanced neuroimaging techniques provide complementary insights: magnetic resonance spectroscopy (MRS) detects regional metabolite concentrations,[17] voxel-based morphometry (VBM) quantifies gray matter volume, and diffusion tensor imaging (DTI) assesses white matter integrity.[18] Resting-state fMRI (rs-fMRI) decodes blood-oxygen-level-dependent (BOLD) fluctuations to dynamically map functional networks, with the Amplitude of Low-Frequency Fluctuations (ALFF) serves as a robust indicator of spontaneous neural activity within specific brain regions,[19] Functional Connectivity (FC) analysis quantifies the temporal coherence between distinct neural regions.[20] The integration of ALFF and FC analyses in rs-fMRI analysis provides a comprehensive framework for understanding disease-related disruptions in brain function across both local and global scales. By integrating bidirectional MR with rs-fMRI network analyses, our study establishes neuroimaging signatures for preclinical DPN detection and redefines therapeutic targets, bridging molecular diabetology and systems neuroscience.

Materials and Methods

GWASs of Brain rs-fMRI and DPN in MR Analysis

This study used rs-fMRI data from Reference,[21] which analyzed associations between 1,777 intrinsic brain activity phenotypes and 9,026,427 genetic variants in the UK Biobank (n = 34,691).[22–24] Of these, 191 phenotypes significantly influenced by genetic variation ($p < 5\times10^{-8}$) were selected, including amplitude features, functional connectivity pairs, and global connectivity measures. Details can be found in the original publication and Supplementary Table 1. GWAS summary statistics of DPN were obtained from FinnGen Biobank (R12 release: 3862 DPN cases:92,612 controls; https://risteys.finngen.fi/endpoints/DM_NEUROPATHY). Significant SNPs ($p < 5\times10^{-6}$) were pruned using a linkage disequilibrium threshold ($R^2 > 0.001$) and filtered to exclude confounding traits. Exposure and outcome data were standardized, and palindromic SNPs were removed. F-statistics (>10) were calculated to ensure robust instrument strength.[25]

Two-Sample MR Analysis Procedure

We performed bidirectional two-sample MR analyses to explore the causal relationships between DPN and rs-fMRI phenotypes. Brain rs-fMRI served as the exposure and DPN as the outcome in forward MR analysis, while DPN were used as exposure and brain rs-fMRI were used as outcome in the reverse MR analyses. The inverse-variance-weighted (IVW) model as the primary method for causal evaluation.[26] Additional methods, including weighted mode, weighted median, MR-Egger regression, and simple mode, were applied for result validation. Odds ratios (ORs) with 95% confidence intervals (CIs) were used to present effect estimates.[27] To reduce horizontal pleiotropy, MR-PRESSO identified outlier instruments, and heterogeneity tests using IVW and MR-Egger regression quantified heterogeneity with Cochran's Q statistics ($P < 0.05$). A leave-one-out analysis assessed result stability by sequentially excluding each SNP.[28] A detailed overview of the process is illustrated in Figure 1.

Study Population in Clinical rs-fMRI Study

We recruited 16 patients with DPN (age 55.88±9.44 years, 5 females), 24 NDPN patients (age 37.88±9.08 years, 5 females), and 20 healthy controls (age 32.25±7.66 years, 9 females) from Renmin Hospital of Wuhan University outpatient clinics between February 2023 and September 2024. This study was approved by the Ethics Committee of Institutional Review Board of Renmin Hospital of Wuhan University (Ethics No.WDRY2024-K220). All participants provided written informed consent, and the research adhered to the principles of the Declaration of Helsinki.

All patients met the 1999 WHO T2DM diagnostic criteria, while DPN diagnosis adhered to the Toronto consensus criteria. Inclusion criteria for patients included age 30–70 years, right-handedness, and at least a junior high school education. NDPN patients had confirmed T2DM but no neuropathic symptoms, normal nerve conduction studies, and

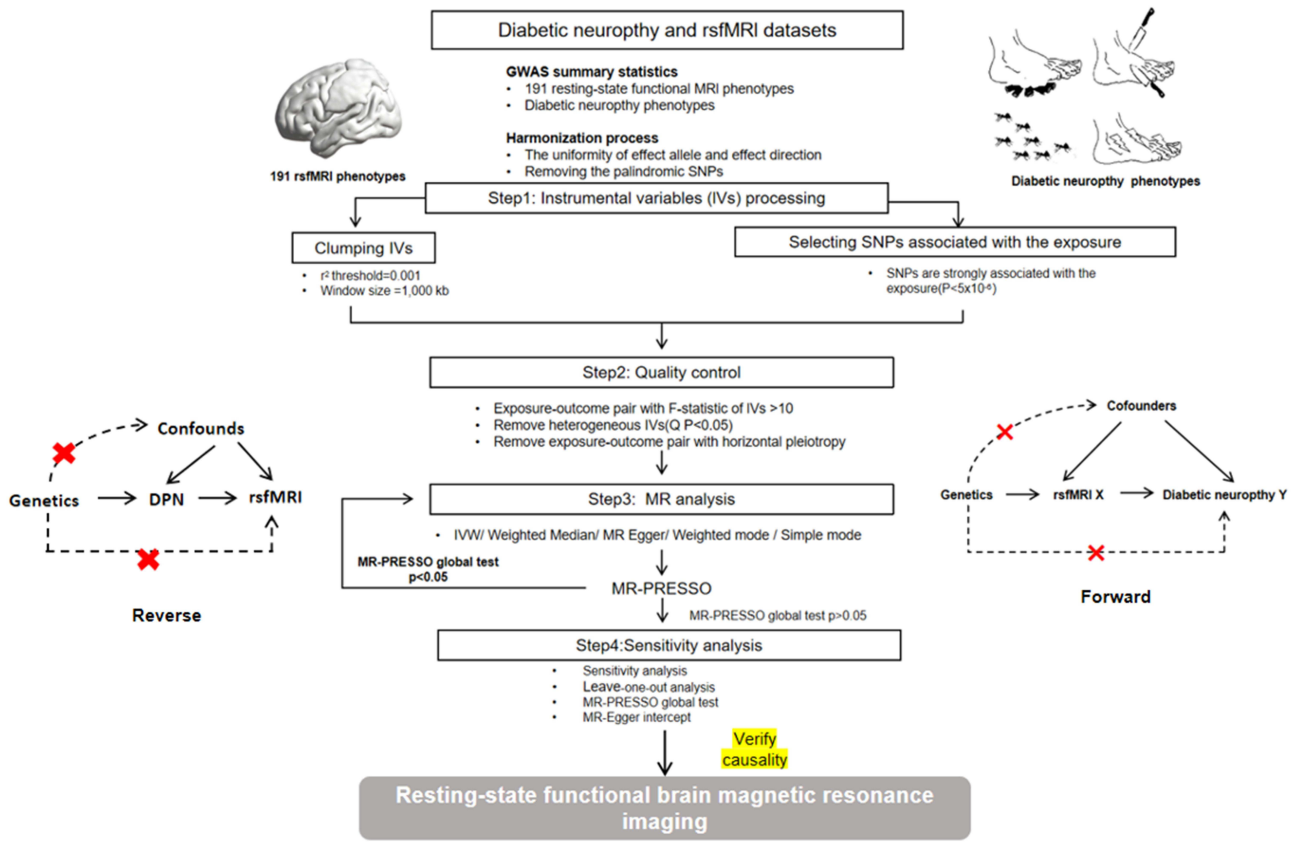

Figure 1 Bidirectional Mendelian Randomization Workflow Between rs-fMRI and DPN. This bidirectional two-sample MR analysis evaluated causal relationships between 191 rs-fMRI phenotypes and DPN. SNPs that were independent and significantly associated with exposure were selected as IVs, and SNPs associated with confounders were discarded. After stringent quality control on IVs, MR analysis was conducted to infer the causality between rs-fMRI phenotype and DPN. Finally, sensitivity analyses were used to assess the robustness of MR inference. Forward and reverse are carried out in the same way.

Abbreviations: DPN, Diabetic Peripheral Neuropathy; rs-fMRI, Resting-state Functional Magnetic Resonance Imaging; GWAS, Genome-Wide Association Study; IVs, Instrumental Variables; MR, Mendelian Randomization; IVW, Inverse Variance Weighted.

exclusion of other neuropathy causes. Healthy controls were aged 30–70 years, right-handed, had no history of diabetes (HbA1c 4–6%), and were free from severe medical, psychiatric, or neurological disorders.

Exclusion criteria encompassed left-handedness, other causes of neuropathy, brain trauma or tumors, acute T2DM complications, cerebrovascular or psychiatric conditions, alcohol or drug abuse, and MRI contraindications.

Clinical Assessment and Questionnaire

First, general data, medical history, and blood biochemical tests were collected from all participants. Then, neurological, psychological, and cognitive assessments were conducted, with the Montreal Cognitive Assessment (MoCA) Beijing version used for a comprehensive evaluation of cognitive function. Next, the Douleur Neuropathique 4(DN4) was used to quantitatively assess the severity of pain. The Visual Function Index-14 (VF-14) questionnaire was used to assess the visual function of patients. All tests were administered by trained and qualified assessors.

rs-fMRI Data Acquisition and Preprocessing

All rs-fMRI scans were obtained on the same GE Discovery MR750w 3.0TMR scanner. The rs-fMRI data were acquired with an echo-planar imaging sequence that included the following parameters—repetition time: TR 2000 ms, TE 25 ms, flip angle 90°, field of view 240 mm×240 mm, number of layers 40, layer thickness 3.5 mm, layer spacing 0.6 mm, matrix 64×64, scanning time about 8 min. During the scan acquisition, the participants were asked to keep their eyes closed, not to think of anything and not to fall asleep.

https://doi.org/10.2147/DMSO.S525219

Spatial preprocessing of rs-fMRI images was conducted using Statistical Parametric Mapping (SPM12, https://www.fil.ion.ucl.ac.uk/spm/software/spm12/). To minimize acquisition delays and head movement artifacts,[29] rs-fMRI images were corrected accordingly. Subjects with head movements exceeding 3 mm or rotations greater than 3°during scanning were excluded from further analysis. The rs-fMRI data were normalized to the standard SPM12 echo planar imaging (EPI) template and resampled to a voxel size of 3 × 3×3 mm^3.[30] To reduce the impact of low-frequency drifts and physiological high-frequency noise, the data were temporally band-pass filtered (0.01–0.08 Hz). Additionally, linear trends were removed, and head movement parameters were regressed out.[31]

ALFF and FC Analysis

The rs-fMRI Data Analysis Toolkit was used to conduct ALFF analysis. Using fast Fourier transform (FFT), the filtered time series was transformed into the frequency domain. The power spectrum was obtained by applying a squared FFT and averaging across the 0.01–0.08 Hz frequency range for each voxel.[19] The square root of the mean power was defined as the ALFF value. A mask based on the Montreal Neurological Institute (MNI) template was created to exclude non-cerebral tissues, ensuring alignment with the normalization procedure. To facilitate inter-subject comparison, ALFF values were normalized by dividing each voxel's ALFF by the whole-brain mean ALFF. Finally, a zALFF map was generated by standardizing ALFF values, subtracting the mean, and dividing by the standard deviation.[20]

Brain regions with altered activity identified through ALFF analysis were selected as seeds for whole-brain FC analysis. Pearson correlation coefficients between each seed and the whole brain were computed, followed by Fisher's Z-transformation for normalization.

rs-fMRI Statistical Analysis

Group differences were assessed using DPABI. A one-way ANCOVA compared ALFF values among the three groups, controlling for age, sex, disease duration, and mean FD. Post hoc analyses with Scheffé correction were performed, and adjusted p-values were converted to z-scores. Significant clusters were identified using FDR correction ($p < 0.05$) and localized with the Automated Anatomical Labeling map. Regions showing significant ALFF differences were selected as seeds for FC analysis.[32] Group-level FC comparisons used ANCOVA, adjusting for age, sex, mean FD, disease duration and cognitive competence, with significant clusters identified using GRF correction (voxel-wise $p < 0.001$, cluster-wise $p < 0.05$).[33,34] Correlations between ALFF of significant brain area and clinical/cognitive variables were also analyzed.

Receiver Operating Characteristic Curve Analysis

ALFF values from the LSFG were extracted after post hoc testing, and receiver operating characteristic (ROC) curves were used to evaluate their potential as neuroimaging biomarkers for distinguishing DPN from NDPN patients. The area under the curve (AUC),[35] maximum Youden index, optimal cutoff point, sensitivity, specificity, and 95% confidence intervals (CIs) were calculated.[36] Statistical comparisons of the AUCs for each mean value were then performed.

Results

Clinical and Neuropsychological Data

Compared to the HC and NDPN groups, the DPN group was older ($p < 0.001$), demonstrated lower cognitive function as assessed by the MoCA ($p < 0.001$), had more severe pain perception ($p < 0.001$), had a longer duration of the disease ($p < 0.001$). Additionally, the DPN group exhibited higher levels of triglycerides (TG) compared to the NDPN group ($p < 0.001$). The demographic details and clinical characteristics of each group are shown in Table 1.

Bidirectional Influences Between Brain Network and DPN in MR Analysis

The full MR analysis results are available in Supplementary Tables S2, S3 and Figure 2. In forward analysis, we identified that a one standard deviation decrease in functional connectivity of default mode network (DMN) and visual network casually corresponds to a 39% increased risk of DPN (IVW OR = 0.61, 95% CI: 0.43–0.86, P = 0.035). In reverse analysis, higher risk of DPN increased the connectivity of the subcortical-cerebellar network (IVW OR = 1.05, 95% CI: 1.01–1.09, P = 0.010). No

Table 1 Demographic and Clinical Characteristics of DPN, NDPN and HC (X±s/ M(P25,P75))

Characteristics	DPN	NDPN	HC	P Value	P Value (Post Hoc)		
					DPN vs HC	DPN vs NDPN	NDPN vs HC
Gender	11 M/5 F	19M/5 F	11 M/9 F	0.057[χ2]	–	–	–
Age, years	55.88± 9.44	37.88±9.08	32.25±7.66	<0.001[a]	<0.001	0.038	<0.001
BMI, kg/m2	23.38±2.89	26.71±3.70	23.09±3.61	0.243[a]			
MoCA	24.69±1.85	26.17±3.54	28.70±1.17	<0.001[a]	<0.001	0.076	0.002
DN4	5.00(4.00,5,75)	0(0.00,0.75)		<0.001[m]			
VF-14	15.50±1.15	13.46±4.07		0.056[b]			
Duration of the disease, years	8.46±5.76	0.36±0.68		<0.001[b]			
HBAlc, %	9.15(7.97,13.63)	11.20(9.28,11.88)		0.448[m]			
TCH, mmol/l	5.01±1.20	4.57±1.04		0.110[b]			
TG, mmol/l	2.61±0.54	1.79±0.22		<0.001[b]			
LDLC, mmol/l	3.32±0.62	2.89±0.74		0.065[b]			
HDLC, mmol/l	0.91±0.28	1.13±0.40		0.064[b]			
c-peptide 0h	1.45±0.68	1.31±0.72		0.537[b]			
c-peptide 2h	4.6±7.07	2.76±1.64		0.225[b]			

Abbreviations: χ2, a:ANOVA test, b: Two-sample *t* test; m: Mann–Whitney test; Data are presented as percentages or means ±SD or, for non-normal distribution, as medians (5th percentile, 95th percentile).

heterogeneity or horizontal pleiotropy was found (Figures 3 and 4). Additional analyses, including forest plots, scatter plots, funnel plots, and leave-one-out analyses, are shown in Supplementary Figures S1 and S2.

Altered Brain Activity Among Groups

After removing age, sex, mean FD, disease duration and cognitive competence as covariates, compared to the NDPN group, the DPN group exhibited a significant increase in the ALFF in left superior frontal gyrus (LSFG, modulates pain and integrates emotions). No significant differences observed between DPN and NDPN groups, NDPN and HC groups. For further details, please refer to Table 2 and Figure 5.

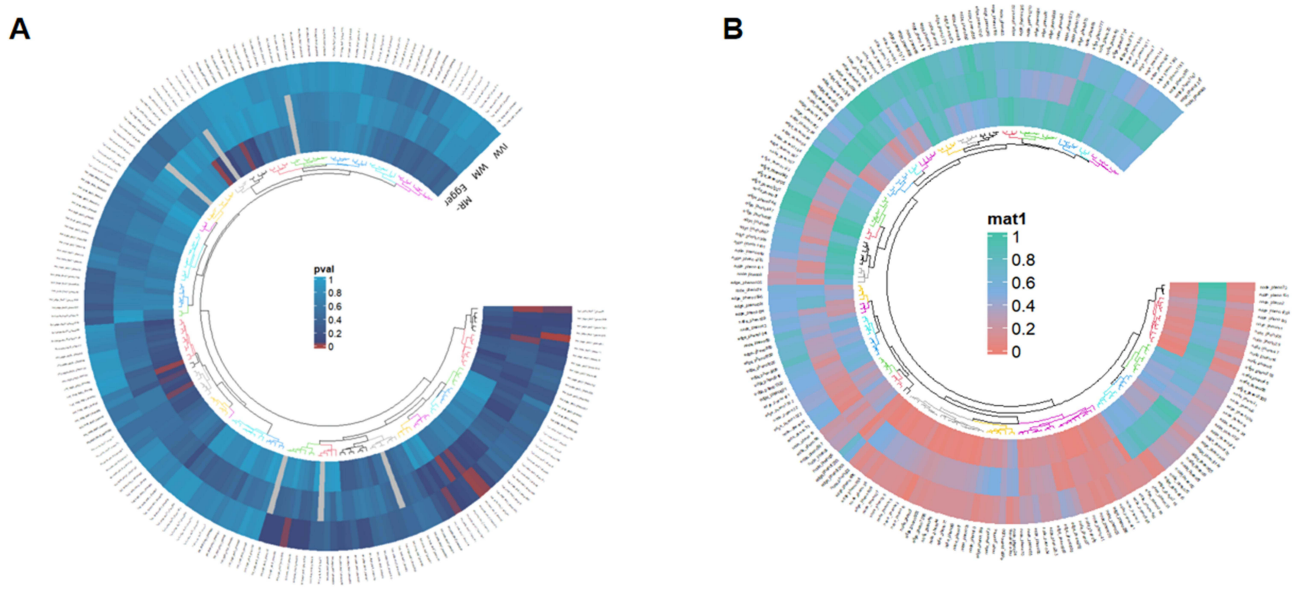

Figure 2 Ring heat map for the MR analysis. (**A**) Forward MR Analysis (rs-fMRI for exposure, DPN for outcome). (**B**) Reverse MR Analysis (DPN for exposure, rs-fMRI for outcome). The causal relationships between 191 rs-fMRI and DPN are illustrated. Each ring represents a different analytical method, and the association between each phenotype and DPN is visualized through variations in color intensity and position.

https://doi.org/10.2147/DMSO.S525219

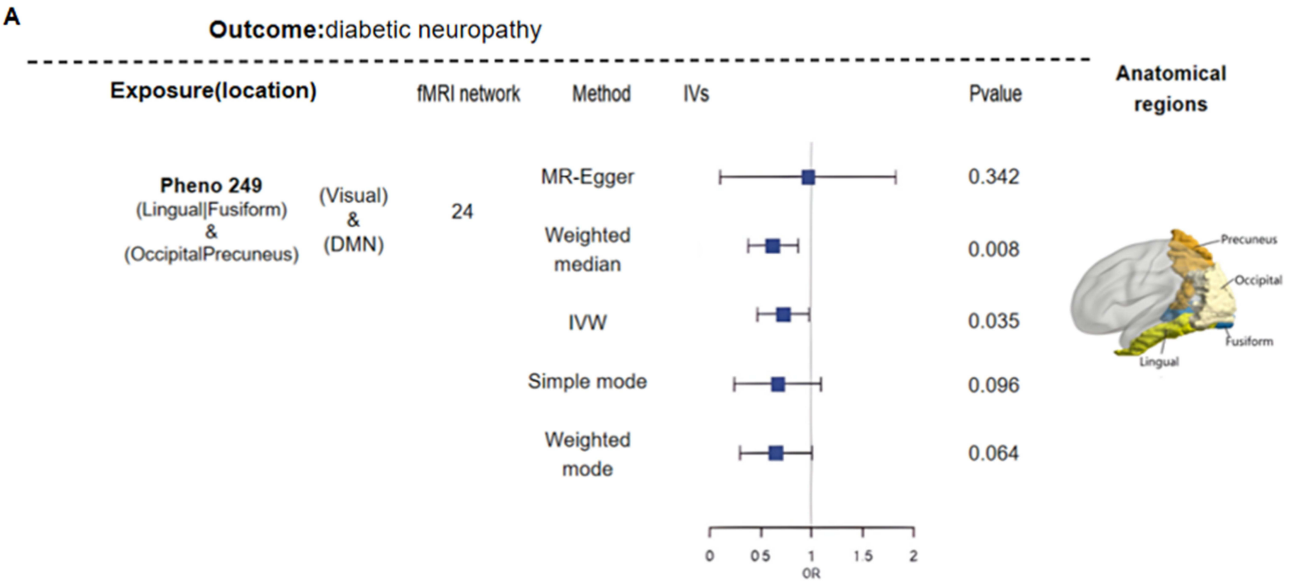

B

Exposure	Outcome	Heterogeneity test			MR-egger pleiotropy test		
		Q	Df	Pvalue	Intercept	SE	Pvalue
Pheno **249**	**DPN**	34.412	23	0.067	0.0237	0.033	0.491

Figure 3 Causalities in the forward MR analysis. (**A**) Forest plots demonstrate significant causal relationships estimated using the five MR Methods. The OR represents the magnitude of the effect on the risk of DPN per 1 standard deviation change in the mean rs-fMRI phenotype, and the error line represents the 95% confidence interval. P values were derived from IVW analyses. Right shows the brain anatomical regions of the corresponding rs-fMRI phenotype. (**B**) Heterogeneity and horizontal pleiotropy analysis of MR analysis.

Correlation Analysis

We conducted a correlation analysis between the ALFF values of the LSFG and clinical indicators as well as scale scores. The ALFF of LSFG was positively correlated with durations of DM ($r = 0.55$ $p = 0.0022$) and negatively correlated with DN-4 ($r = -0.47$, $p = 0.0024$). The details are shown in Supplementary Figure S3.

ROC Curve Analysis Results

According to the ROC curves, the mean ALFF values of the LSFG can distinguish DPN from patients with NDPN, which all achieved a significance level of $P<0.05$ for AUC. An AUC of 0.79 indicates a moderately performing classifier, demonstrating a certain level of predictive value. The details are shown in Figure 6.

Functional Connectivity Analysis

Compared to the HC group, the DPN group exhibited decreased FC between LSFG and right lingual (LING.R, basic visual feature processing). Conversely, FC between the LSFG and right precuneus (PCUN.R, complex visuospatial processing, visual input integration, and episodic memory within the DMN) increased. No significant changes were observed in DPN and NDPN groups, NDPN and HC groups. Shown in Table 3 and Figure 7.

Discussion

This study identified altered intrinsic brain activity in DPN patients, characterized by abnormal ALFF and distinct FC patterns in emotional and visual processing regions. Notably, elevated ALFF in the LSFG emerged as a potential neuroimaging biomarker for DPN. To our knowledge, this represents the first integration of Mendelian randomization

A

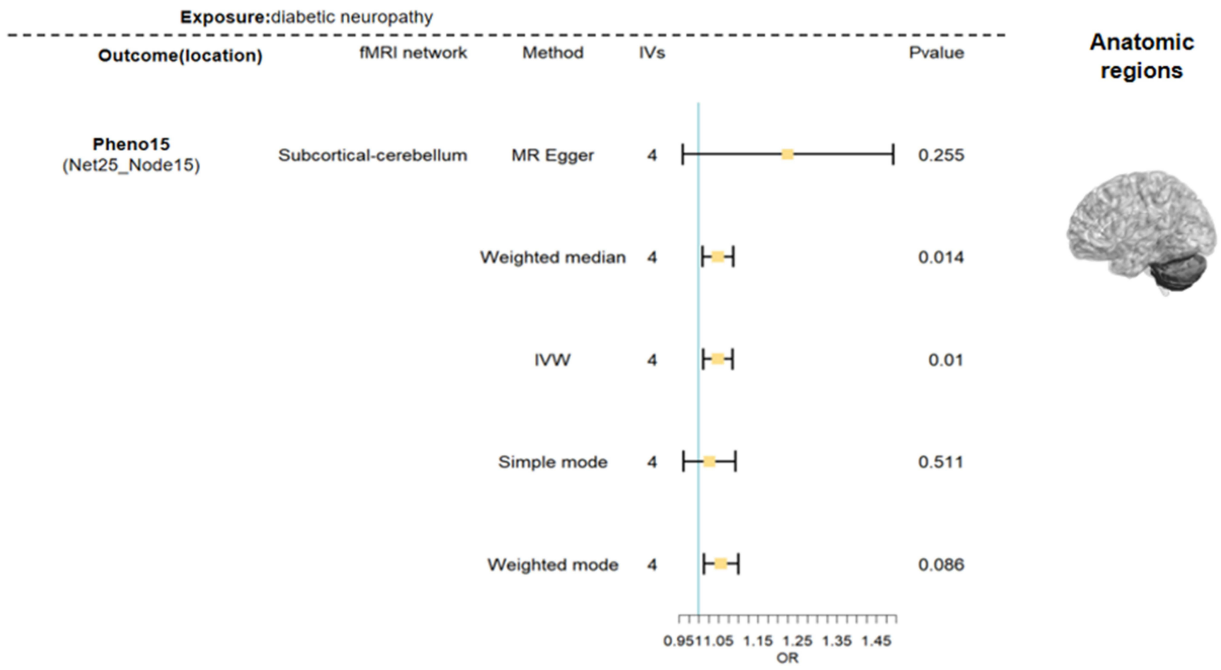

B

Outcome	Exposure	Heterogeneity test			MR-egger pleiotropy test		
		Q	Df	Pvalue	Intercept	SE	Pvalue
Pheno **15**	**DPN**	2.515	3	0.47	-0.044	0.037	0.357

Figure 4 Causalities in the Reverse MR analysis. (**A**) Forest plots demonstrate significant causal relationships estimated using the five MR Methods. The OR represents the magnitude of the effect on the risk of rs-fMRI per 1 standard deviation change in the mean DPN phenotype, and the error line represents the 95% confidence interval. P values were derived from IVW analyses. Right shows the brain anatomical regions of the corresponding rs-fMRI phenotype. (**B**) Heterogeneity and horizontal pleiotropy analysis of MR analysis.

with clinical resting-state fMRI, enabling comprehensive exploration of regional brain alterations and the "metabolism-neurodegeneration-compensation imbalance" cycle in DPN.

Significant age differences between groups reflected longer disease duration and more frequent neurological screening in elderly patients.[37] The DPN group showed higher DN4 scores and lower MoCA scores, indicating greater pain severity and cognitive impairment that may indirectly contribute to negative emotional states.[38] To address this demographic heterogeneity, we included age and cognitive function as a covariate to remove in subsequent analyses. Elevated triglyceride (TG) levels in DPN patients align with preclinical evidence linking TG overload to impaired nerve metabolism and mitochondrial dysfunction.[39] These findings align with results from a Danish cohort study that demonstrated a significant association between elevated triglycerides and increased DPN risk.[40]

Forward MR demonstrated that reduced DMN-visual connectivity increases DPN risk. The DMN supports environmental monitoring, emotional processing, and self-referential cognition,[41,42] while the visual network coordinates visual perception.[43] Notably, Both networks contain NMDAR-GLUT1 co-expressing neurons highly vulnerable to

Table 2 ALFF Values Were Significantly Different Between Groups (P <0.05 After FDR Correction Using ANCOVA and Sheffe Post Hoc Tests)

Condition	Brain Area	BA	Cluster Size	MNI			Peak t Score
				x	y	z	
DPN>NDPN	LSFG	BA9_L	61	−6	45	51	5.28884

Abbreviation: LSFG, left superior frontal gyrus.

https://doi.org/10.2147/DMSO.S525219

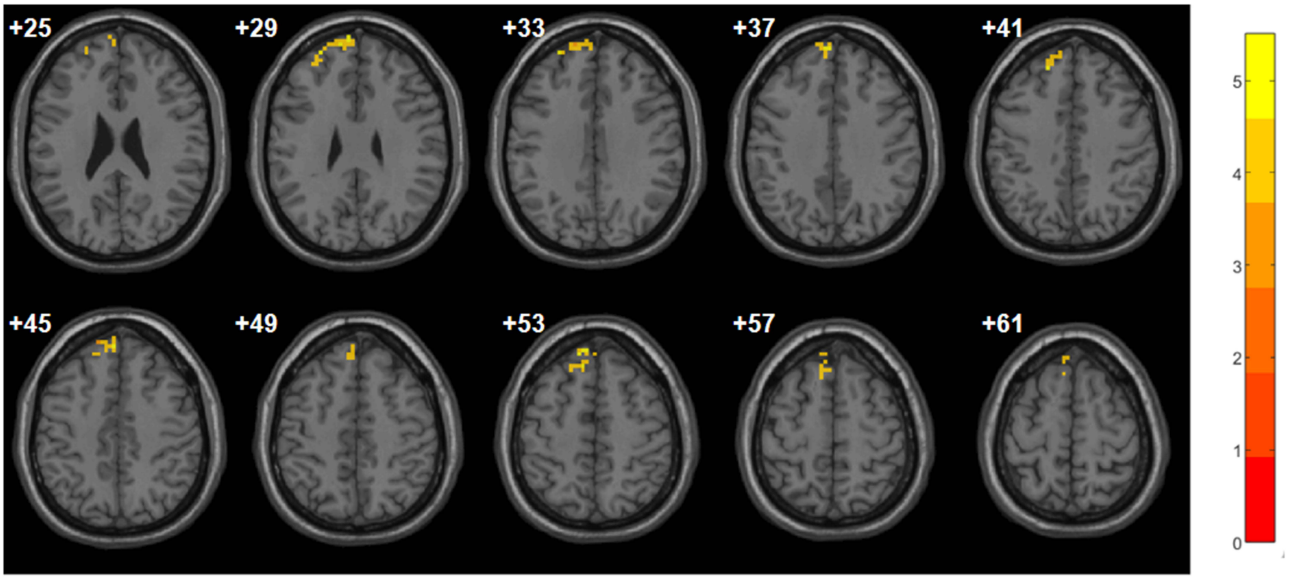

Figure 5 Clusters of significant changes in ALFF values among groups (analyzed using analysis of covariance (ANCOVA) and Scheffé post hoc tests, with FDR correction, P <0.05). Red regions (LSFG, left superior frontal gyrus) indicate that the DPN group has higher ALFF values compared to the HC group.

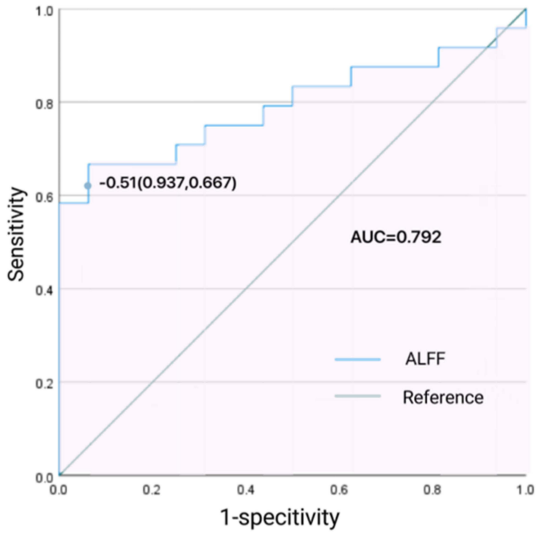

	P value	Cutoff value	SENSITIVITY	SPECIFICITY	AUC	95% CI
ALFF_LSFG	0.02	-0.51	0.667	0.037	0.792	0.651-0.993

Figure 6 ROC curves for ALFF that distinguish patients with NDPN from patients with DPN and controls. The AUC of "ALFF_LSFG" index was 0.792, which had moderate diagnostic performance.
Abbreviations: ALFF, amplitude of low-frequency fluctuation; AUC, area under the curve; LSFG, left superior frontal gyrus.

glycoxidative stress-induced mitochondrial damage.[44] This connectivity disruption may impair visual processing, spatial orientation, and attentional allocation - consistent with findings in other chronic pain conditions.[45,46] Our results suggest network-specific dysconnectivity acts as a causal driver rather than mere consequence of DPN progression.

Reverse MR revealed that genetic DPN risk enhances subcortical-cerebellar connectivity. Peripheral sensory deafferentation likely triggers cerebellar compensation for degraded proprioceptive inputs.[47] Subcortical-cerebellar circuits also exhibit abnormal connectivity in psychosis, potentially associated with cognitive dysfunction, positive symptoms (e.g.hallucinations, delusions) and negative symptoms (eg social withdrawal, lack of motivation).[48] Thus, this compensatory mechanism may paradoxically amplifies error prediction signals and ultimately leads to maladaptive cortical reorganization, even mental illness.

The DPN group demonstrated significantly elevated ALFF values in the LSFG, a region integral to top-down pain inhibition modulation,[49] previously implicated in both chronic neuropathic pain conditions and severe ocular pain

Table 3 FC Values Were Significantly Different Between Groups, Seed as LSFG

Connectivity Contrast	Seed	Connected Regions	Peak MNI Coordinates			Voxels (mm^3)	BA	Peak Intensity
			X	Y	Z			
DPN>HC	LSFG	Precuneus_R	12	−63	27	405	BA23_R	3.891
DPN<HC	LSFG	Lingual_R	0	−93	−18	351	None	−4.516

Notes: ANCOVA and sheffe post hoc tests with GRF multiple correction were used, voxel p value<0.001, cluster p value<0.05, two tailed.
Abbreviations: LSFG, left superior frontal gyrus; Precuneus_R, right precuneus; Lingual_R, right lingual.

manifestations.[50] The LSFG serves as a critical hub for integrating emotional inputs with environmental stimuli.[51,52] An Italian cohort study, which identified pain unpredictability and reduced pain control as primary contributors to depression in DPN patients.[4] Additionally, DPN patients commonly experience anxiety related to disease progression, potential injury, and perceived social stigma.[43] Thus, the observed heightened LSFG activity may represent a dual mechanism: enhanced nociceptive processing coupled with an adaptive response for managing the emotional and cognitive challenges associated with the condition.[53] The positive ALFF-duration correlation suggests progressive exacerbation of negative emotions. Importantly, ROC analysis confirmed LSFG ALFF effectively discriminates DPN from non-DPN diabetics (AUC=0.79), supporting its utility as a non-invasive neuroplasticity biomarker.

Subsequently, using the LSFG as a seed region, we assessed whole-brain functional connectivity. Compared to the HC group, the DPN group exhibited decreased FC between the LSFG and the LING.R. The lingual gyrus primarily supports basic visual feature processing, including shape, color, and letter recognition.[54] Previous research has documented reduced brain activity in the lingual gyrus among T2DM patients, with cognitive impairment notably preceding the onset of visual dysfunction,[55] which is consistent with our MR Study in the previous part. We hypothesize that this decline may result from attentional reallocation, where the brain prioritizes pain regulation and emotional processing, thereby reducing connectivity with visual areas.[56] Additionally, this may represent an adaptive protective segregation mechanism, in which the brain actively downregulates synchronization with non-essential visual input to minimize interference with critical emotional and pain regulatory processes.

In contrast, increased FC between the LSFG and the PCUN.R was observed in DPN patients. Notably, the precuneus has traditionally been considered a visual region involved in complex visuospatial processing and integrating visual

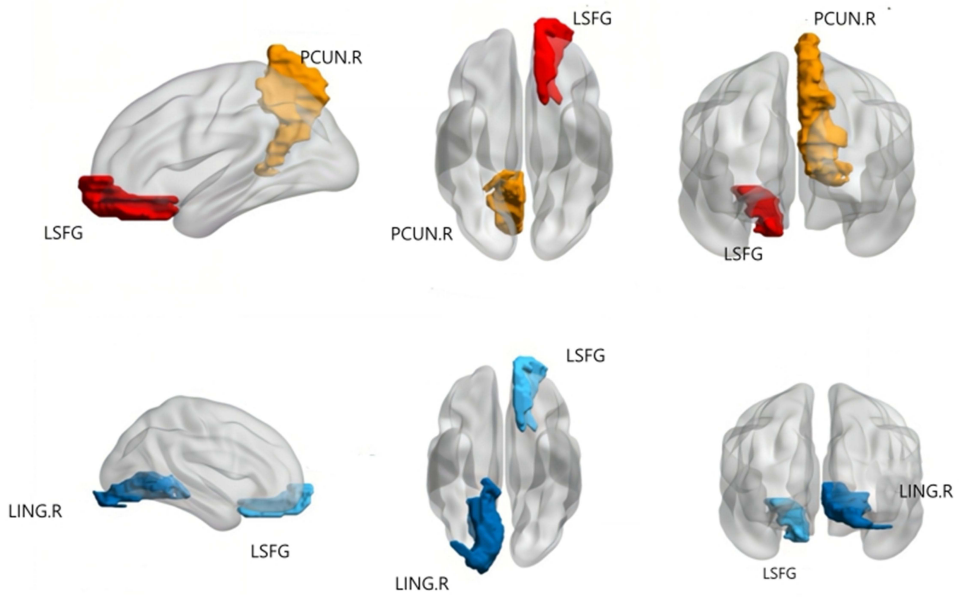

Figure 7 Brain regions with significantly different FC using LSFG as seed points. LSFG has an increased connection to PCUN.R and a decreased connection to LING.R.
Abbreviations: LSFG, left superior frontal gyrus; PCUN.R, right precuneus; LING.R, right lingual gyrus.

https://doi.org/10.2147/DMSO.S525219

inputs.[57] Additionally, it serves as a key hub of the DMN, associated with episodic memory and visuospatial imagery.[58] Enhanced inter-DMN functional connectivity in painful DPN has been already demonstrated,[59] and alterations in the connectivity of the precuneus have been observed in depression and bipolar disorder.[60,61] We propose that this enhanced FC may represent a compensatory mechanism in DPN patients with visual deficits. These patients may rely more heavily on available contextual cues, such as facial expressions and social interactions,[62] and potentially employ mental imagery to infer and compensate for visual impairments.[63] However, research has shown that prolonged negative self-consciousness activates the precuneus,[64] which is associated with the onset of anxiety and depression. Therefore, the chronic enhancement of connectivity between these regions may potentially increasing psychiatric vulnerability.

Combined MR analysis and rs-fMRI, we propose the following hypothesis: hyperglycemia genetically impairs metabolically sensitive DMN-visual network connections, disrupting the integration of basic visual processing (as evidenced by forward MR results) and higher-order spatial conformation. During the early compensatory phase, loss of peripheral sensory neurons triggers enhanced FC between the cerebellum and thalamus via the spinocerebellar tract (as shown by reverse MR results), which rapidly recalibrates motor output. Concurrently, increased ALFF in the LSFG may reflect cognitive inhibition of aberrant sensory inputs by the prefrontal cortex (eg, pain modulation). In the late maladaptive phase, chronic enhancement of hyperconnectivity between the superior frontal gyrus and precuneus may lead to DMN encroachment, resulting in excessive precuneus involvement in visual scenario simulation (as a compensatory substitute for impaired real-time visual processing), may interferes with sensory-motor integration efficiency, perpetuating a vicious cycle of "metabolic dysfunction-neurodegeneration-dysregulated compensation."

This study has several limitations. First, demographic differences among groups in gender ratio, age, and disease duration, while controlled for as covariates, suggest the need for better-matched participants. Second, the small sample size and cross-sectional design limit our understanding of dynamic brain activity changes in DPN, necessitating larger, longitudinally studied cohorts. Third, medication effects on neural activity warrant future studies focusing on drug-naïve patients. Fourth, the predominantly European GWAS dataset requires validation in other populations. Finally, while genetic variations parallel environmental factors, they may not fully replicate environmental changes, potentially biasing MR analysis results and requiring further clinical validation.

Conclusions

This study integrates MR with rs-fMRI to systematically elucidate the cross-scale network reorganization mechanisms underlying DPN. Key findings include that changes in LSFG may serve as a potential neuroimaging biomarker for DPN diagnosis, reflecting abnormalities in pain and emotional processing. The reduction in DMN-visual network functional connectivity is identified as a causal driver of DPN onset, while DPN genetic risk achieves central compensation by enhancing subcortical-cerebellar functional connectivity. Resting-state functional imaging reveals dynamic network remodeling in DPN patients: increased spontaneous neural activity (ALFF) in the superior frontal gyrus and decreased functional connectivity with the lingual gyrus reflect metabolic attacks on primary visual pathways, while elevated connectivity with the precuneus suggests higher-order cognitive networks recruit spatial memory to compensate for impaired visual input. This "metabolic injury-compensatory remodeling" pattern reveals DPN's pathological evolution from central to peripheral systems and provides clinical research with novel biomarkers and intervention targets.

Author Contributions

All authors contributed to study conception, design, and data acquisition/analysis; participated in manuscript preparation and critical editing; approved the final version; endorsed journal selection; and accept full responsibility for the work.

Funding

This study was supported by National Science Foundation of China (Project # 82270861 to Dr. Gao), the Fundamental Research Funds for the Central Universities (Project # 2042020kf1079 to Dr. Gao), China International Medical Foundation (Project #2018HX0003) and the Planned international development Project of Wuhan University.

Disclosure

The authors report no conflicts of interest in this work.

References

1. Alharajin RS, Al Moaibed HS, Al Khalifah FK. Prevalence of painful diabetic peripheral neuropathy among Saudi patients with diabetes in Al Ahsa: a Cross-sectional study. *Cureus*. 2023;15(11):e49317. doi:10.7759/cureus.49317
2. Nabavi Nouri M, Ahmed A, Bril V, et al. Diabetic neuropathy and axon reflex-mediated neurogenic vasodilatation in type 1 diabetes. *PLoS One*. 2012;7(4):e34807. doi:10.1371/journal.pone.0034807
3. Abbott CA, Malik RA, van Ross ERE, Kulkarni J, Boulton AJM. Prevalence and characteristics of painful diabetic neuropathy in a large community-based diabetic population in the U.K. *Diabetes Care*. 2011;34(10):2220–2224. doi:10.2337/dc11-1108
4. Naranjo C, Del Reguero L, Moratalla G, Hercberg M, Valenzuela M, Failde I. Anxiety, depression and sleep disorders in patients with diabetic neuropathic pain: a systematic review. *Expert Rev Neurother*. 2019;19(12):1201–1209. doi:10.1080/14737175.2019.1653760
5. Meacham K, Shepherd A, Mohapatra DP, Haroutounian S. Neuropathic pain: central vs. peripheral mechanisms. *Curr Pain Headache Rep*. 2017;21(6):28. doi:10.1007/s11916-017-0629-5
6. Baskozos G, Themistocleous AC, Hebert HL, et al. Classification of painful or painless diabetic peripheral neuropathy and identification of the most powerful predictors using machine learning models in large cross-sectional cohorts. *BMC Med Inf Decis Making*. 2022;22(1):144. doi:10.1186/s12911-022-01890-x
7. Croosu SS, Røikjer J, Mørch CD, Ejskjaer N, Frøkjær JB, Hansen TM. Alterations in functional connectivity of thalamus and primary somatosensory cortex in painful and painless diabetic peripheral neuropathy. *Diabetes Care*. 2023;46(1):173–182. doi:10.2337/dc22-0587
8. Bushnell MC, Duncan GH, Hofbauer RK, Ha B, Chen JI, Carrier B. Pain perception: is there a role for primary somatosensory cortex? *Proc Natl Acad Sci U S A*. 1999;96(14):7705–7709. doi:10.1073/pnas.96.14.7705
9. Kanda M, Nagamine T, Ikeda A, et al. Primary somatosensory cortex is actively involved in pain processing in human. *Brain Res*. 2000;853(2):282–289. doi:10.1016/s0006-8993(99)02274-x
10. Gella L, Pal SS, Ganesan S, Sharma T, Raman R. Foveal slope measurements in diabetic retinopathy: can it predict development of sight-threatening retinopathy? Sankara nethralaya diabetic retinopathy epidemiology and molecular genetics study (SN-DREAMS II, report no 8). *Indian J Ophthalmol*. 2015;63(6):478–481. doi:10.4103/0301-4738.162578
11. Neriyanuri S, Pardhan S, Gella L, et al. Retinal sensitivity changes associated with diabetic neuropathy in the absence of diabetic retinopathy. *Br J Ophthalmol*. 2017;101(9):1174–1178. doi:10.1136/bjophthalmol-2016-309641
12. Bagheri J, Fallahnezhad S, Alipour N, et al. Maternal diabetes decreases the expression of α2-adrenergic and M2 muscarinic receptors in the visual cortex of male rat neonates. *J Chem Neuroanat*. 2023;132:102326. doi:10.1016/j.jchemneu.2023.102326
13. Ebrahimi M, Thompson P, Lauer AK, Sivaprasad S, Perry G. The retina-brain axis and diabetic retinopathy. *Eur J Ophthalmol*. 2023;33(6):2079–2095. doi:10.1177/11206721231172229
14. Tsoi AT, Sng J, Tummanapalli SS, et al. Metformin therapy modifies corneal neuroimmune abnormalities in people with type 2 diabetes. *Diabetologia*. 2025;68(6):1329–1334. doi:10.1007/s00125-025-06399-2
15. Birney E. Mendelian Randomization. *Cold Spring Harb Perspect Med*. 2022;12(4):a041302. doi:10.1101/cshperspect.a041302
16. Pop-Busui R, Ang L, Boulton AJM, et al. *Diagnosis and Treatment of Painful Diabetic Peripheral Neuropathy*. American Diabetes Association; 2022.
17. Evans MC, Wade C, Hohenschurz-Schmidt D, et al. Magnetic resonance imaging as a biomarker in diabetic and HIV-associated peripheral neuropathy: a systematic review-based narrative. *Front Neurosci*. 2021;15:727311. doi:10.3389/fnins.2021.727311
18. Manu G, Amit M, Asir John S. Effect of massage, passive neural mobilization and transcutaneous electrical nerve stimulation on magnetic resonance diffusion tensor imaging (MR-DTI) of the tibial nerve in a patient with type 2 diabetes mellitus induced neuropathy: a case report. *Physiother Theory Pract*. 2022;38(13):3273–3282. doi:10.1080/09593985.2021.1994070
19. Zou QH, Zhu CZ, Yang Y, et al. An improved approach to detection of amplitude of low-frequency fluctuation (ALFF) for resting-state fMRI: fractional ALFF. *J Neurosci Methods*. 2008;172(1):137–141. doi:10.1016/j.jneumeth.2008.04.012
20. Biswal B, Yetkin FZ, Haughton VM, Hyde JS. Functional connectivity in the motor cortex of resting human brain using echo-planar MRI. *Magn Reson Med*. 1995;34(4):537–541. doi:10.1002/mrm.1910340409
21. Zhao B, Li T, Smith SM, et al. Common variants contribute to intrinsic human brain functional networks. *Nat Genet*. 2022;54(4):508–517. doi:10.1038/s41588-022-01039-6
22. Elliott LT, Sharp K, Alfaro-Almagro F, et al. Genome-wide association studies of brain imaging phenotypes in UK biobank. *Nature*. 2018;562(7726):210–216. doi:10.1038/s41586-018-0571-7
23. Grasby KL, Jahanshad N, Painter JN, et al. The genetic architecture of the human cerebral cortex. *Science*. 2020;367(6484):eaay6690. doi:10.1126/science.aay6690
24. Selvarajah D, Sloan G, Teh K, et al. Structural brain alterations in key somatosensory and nociceptive regions in diabetic peripheral neuropathy. *Diabetes Care*. 2023;46(4):777–785. doi:10.2337/dc22-1123
25. Pierce BL, Burgess S. Efficient design for Mendelian randomization studies: subsample and 2-sample instrumental variable estimators. *Am J Epidemiol*. 2013;178(7):1177–1184. doi:10.1093/aje/kwt084
26. Burgess S, Thompson SG; CRP CHD Genetics Collaboration. Avoiding bias from weak instruments in Mendelian randomization studies. *Int J Epidemiol*. 2011;40(3):755–764. doi:10.1093/ije/dyr036
27. Winsløw UC, Nordestgaard BG, Afzal S. High plasma 25-hydroxyvitamin D and high risk of nonmelanoma skin cancer: a Mendelian randomization study of 97 849 individuals. *Br J Dermatol*. 2018;178(6):1388–1395. doi:10.1111/bjd.16127
28. Chen Y, Chen W. Genome-wide integration of genetic and genomic studies of atopic dermatitis: insights into genetic architecture and pathogenesis. *J Invest Dermatol*. 2022;142(11):2958–2967.e8. doi:10.1016/j.jid.2022.04.021
29. Friston KJ, Williams S, Howard R, Frackowiak RS, Turner R. Movement-related effects in fMRI time-series. *Magn Reson Med*. 1996;35(3):346–355. doi:10.1002/mrm.1910350312
30. Jenkinson M, Bannister P, Brady M, Smith S. Improved optimization for the robust and accurate linear registration and motion correction of brain images. *Neuroimage*. 2002;17(2):825–841. doi:10.1016/s1053-8119(02)91132-8
31. Ashburner J. A fast diffeomorphic image registration algorithm. *NeuroImage*. 2007;38(1):95–113. doi:10.1016/j.neuroimage.2007.07.007
32. Glickman ME, Rao SR, Schultz MR. False discovery rate control is a recommended alternative to Bonferroni-type adjustments in health studies. *J Clin Epidemiol*. 2014;67(8):850–857. doi:10.1016/j.jclinepi.2014.03.012

33. Bansal R, Peterson BS. Cluster-level statistical inference in fMRI datasets: the unexpected behavior of random fields in high dimensions. *Magn Reson Imaging*. 2022;87:19–31. doi:10.1016/j.mri.2021.12.001
34. Agziyart EA, Abbasian K, Makouei S, Mohammadi SB. Investigating changes of functional brain networks in major depressive disorder by graph theoretical analysis of resting-state fMRI. *Psychiatry Res Neuroimaging*. 2024;344:111880. doi:10.1016/j.pscychresns.2024.111880
35. Perkins NJ, Schisterman EF. The youden index and the optimal cut-point corrected for measurement error. *Biom J*. 2005;47(4):428–441. doi:10.1002/bimj.200410133
36. Faraggi D, Reiser B. Estimation of the area under the ROC curve. *Stat Med*. 2002;21(20):3093–3106. doi:10.1002/sim.1228
37. Sloan G, Selvarajah D, Tesfaye S. Pathogenesis, diagnosis and clinical management of diabetic sensorimotor peripheral neuropathy. *Nat Rev Endocrinol*. 2021;17(7):400–420. doi:10.1038/s41574-021-00496-z
38. Tesfaye S, Sloan G, Petrie J, et al. Comparison of amitriptyline supplemented with pregabalin, pregabalin supplemented with amitriptyline, and duloxetine supplemented with pregabalin for the treatment of diabetic peripheral neuropathic pain (OPTION-DM): a multicentre, double-blind, randomised crossover trial. *Lancet*. 2022;400(10353):680–690. doi:10.1016/S0140-6736(22)01472-6
39. Vincent AM, Hayes JM, McLean LL, Vivekanandan-Giri A, Pennathur S, Feldman EL. Dyslipidemia-induced neuropathy in mice: the role of oxLDL/LOX-1. *Diabetes*. 2009;58(10):2376–2385. doi:10.2337/db09-0047
40. Kristensen FPB, Christensen DH, Callaghan BC, et al. Lipid levels and risk of diabetic polyneuropathy in 2 Danish type 2 diabetes cohorts. *Neurology*. 2024;103(1):e209538. doi:10.1212/WNL.0000000000209538
41. Cui Y, Jiao Y, Chen HJ, et al. Aberrant functional connectivity of default-mode network in type 2 diabetes patients. *Eur Radiol*. 2015;25(11):3238–3246. doi:10.1007/s00330-015-3746-8
42. Tesfaye S, Selvarajah D, Gandhi R, et al. Diabetic peripheral neuropathy may not be as its name suggests: evidence from magnetic resonance imaging. *Pain*. 2016;157(Suppl 1):S72–S80. doi:10.1097/j.pain.0000000000000465
43. Pouwer F, Mizokami-Stout K, Reeves ND, et al. Psychosocial care for people with diabetic neuropathy: time for action. *Diabetes Care*. 2024;47(1):17–25. doi:10.2337/dci23-0033
44. Saab AS, Tzvetavona ID, Trevisiol A, et al. Oligodendroglial NMDA receptors regulate glucose import and axonal energy metabolism. *Neuron*. 2016;91(1):119–132. doi:10.1016/j.neuron.2016.05.016
45. Shen W, Tu Y, Gollub RL, et al. Visual network alterations in brain functional connectivity in chronic low back pain: a resting state functional connectivity and machine learning study. *Neuroimage Clin*. 2019;22:101775. doi:10.1016/j.nicl.2019.101775
46. Schwedt TJ, Schlaggar BL, Mar S, et al. Atypical resting-state functional connectivity of affective pain regions in chronic migraine. *Headache*. 2013;53(5):737–751. doi:10.1111/head.12081
47. Thach WT, Goodkin HP, Keating JG. The cerebellum and the adaptive coordination of movement. *Annu Rev Neurosci*. 1992;15:403–442. doi:10.1146/annurev.ne.15.030192.002155
48. Jensen KM, Calhoun VD, Fu Z, et al. A whole-brain neuromark resting-state fMRI analysis of first-episode and early psychosis: evidence of aberrant cortical-subcortical-cerebellar functional circuitry. *Neuroimage Clin*. 2024;41:103584. doi:10.1016/j.nicl.2024.103584
49. Schmahl CG, Vermetten E, Elzinga BM, Bremner JD. A positron emission tomography study of memories of childhood abuse in borderline personality disorder. *Biol Psychiatry*. 2004;55(7):759–765. doi:10.1016/j.biopsych.2003.11.007
50. Yu C, Li CQ, Ge QM, et al. Altered resting state functional activity of brain regions in neovascular glaucoma: a resting-state functional magnetic resonance imaging study. *Front Neurosci*. 2021:15. doi:10.3389/fnins.2021.800466
51. du Boisgueheneuc F, Levy R, Volle E, et al. Functions of the left superior frontal gyrus in humans: a lesion study. *Brain*. 2006;129(Pt 12):3315–3328. doi:10.1093/brain/awl244
52. Wang S, Zhao Y, Zhang L, et al. Stress and the brain: perceived stress mediates the impact of the superior frontal gyrus spontaneous activity on depressive symptoms in late adolescence. *Hum Brain Mapp*. 2019;40(17):4982–4993. doi:10.1002/hbm.24752
53. Buckner RL, Andrews-Hanna JR, Schacter DL. The brain's default network: anatomy, function, and relevance to disease. *Ann N Y Acad Sci*. 2008;1124:1–38. doi:10.1196/annals.1440.011
54. Palejwala AH, Dadario NB, Young IM, et al. Anatomy and white matter connections of the lingual gyrus and cuneus. *World Neurosurg*. 2021;151:e426–e437. doi:10.1016/j.wneu.2021.04.050
55. Salido EM, de Zavalía N, Schreier L, et al. Retinal changes in an experimental model of early type 2 diabetes in rats characterized by non-fasting hyperglycemia. *Exp Neurol*. 2012;236(1):151–160. doi:10.1016/j.expneurol.2012.04.010
56. Santos-Mayo A, Moratti S. How fear conditioning affects the visuocortical processing of context cues in humans. Evidence from steady state visual evoked responses. *Cortex*. 2024;183:21–37. doi:10.1016/j.cortex.2024.11.005
57. Horiguchi H, Wandell BA, Winawer J. A predominantly visual subdivision of the right temporo-parietal junction (vTPJ). *Cereb. Cortex*. 2016;26(2):639–646. doi:10.1093/cercor/bhu226
58. Dadario NB, Sughrue ME. The functional role of the precuneus. *Brain*. 2023;146(9):3598–3607. doi:10.1093/brain/awad181
59. Selvarajah D, Wilkinson ID, Maxwell M, et al. Magnetic resonance neuroimaging study of brain structural differences in diabetic peripheral neuropathy. *Diabetes Care*. 2014;37(6):1681–1688. doi:10.2337/dc13-2610
60. Zhu Y, Tang Y, Zhang T, et al. Reduced functional connectivity between bilateral precuneus and contralateral parahippocampus in schizotypal personality disorder. *BMC Psychiatry*. 2017;17(1):48. doi:10.1186/s12888-016-1146-5
61. Tesli M, Kauppi K, Bettella F, et al. Altered brain activation during emotional face processing in relation to both diagnosis and polygenic risk of bipolar disorder. *PLoS One*. 2015;10(7):e0134202. doi:10.1371/journal.pone.0134202
62. Stuhrmann A, Suslow T, Dannlowski U. Facial emotion processing in major depression: a systematic review of neuroimaging findings. *Biol Mood Anxiety Disord*. 2011;1(1):10. doi:10.1186/2045-5380-1-10
63. Ren W, Wang M, Wang Q, et al. Altered functional connectivity in patients with post-stroke fatigue: a resting-state fMRI study. *J Affect Disord*. 2024;350:468–475. doi:10.1016/j.jad.2024.01.129
64. Boes AD, Prasad S, Liu H, et al. Network localization of neurological symptoms from focal brain lesions. *Brain*. 2015;138(Pt 10):3061–3075. doi:10.1093/brain/awv228